SOME OTHER GRATINGS: BENCHMARKS FOR LARGE-AREA E-BEAM NANOPATTERNING

Petr MELUZÍN, Miroslav HORÁČEK, Michal URBÁNEK, Jan BOK,
Stanislav KRÁTKÝ, Milan MATĚJKA, Jana CHLUMSKÁ, Vladimír KOLAŘÍK

Institute of Scientific Instruments ASCR, v. v. i., Královopolská 147, CZ–612 64 Brno, Czech Republic
Petr.Meluzin@isibrno.cz

Abstract

E-beam lithography is a flexible technology for diffraction gratings origination. Nevertheless, requirements of the high optical quality of large area diffractive structures imply various severe challenges to e-beam delineating processes. This paper summarizes the e-beam process parameters that influence the quality of large area grating structures. Next, we propose some new methods to prepare diffraction gratings that were found to be useful for testing and benchmarking purposes. Those methods include single line gratings, labyrinth structures, fractional structures, tiling patterns, quasi regular filling structures and forked line structures. Various samples were prepared with the standard and newly developed e-beam patterning processes using both e-beam writers available: one with the Gaussian beam at 100 keV and another one with the shaped beam at 15 keV. Some of the results are presented further in this paper, their variants and parameters are discussed as well as their usefulness as benchmarking e-beam patterns for large area optical structures, elements and devices.

Key words: e-beam writer; optical nano structures, diffraction gratings; fractal gratings

1. INTRODUCTION

An introduction to e-beam patterning technology can be found in e.g. [1] or [2] together with basic testing approaches. The delineating of large-area diffractive patterns introduces special requirements to the quality of field stitching, long-term stability. Those requirements are even more crucial when the greyscale lithography is adopted (instead of the binary masking lithography) and when the required deepness of relief increases. Next, the patterning throughput is of high interest and enhanced patterning strategies (e.g. [3]) are to be adopted. Further parameters include variable-size e-beam stamp homogeneity [4], efficiency of proximity effect simulation and correction algorithms [5], [6], [7], ultimate achievable resolution [8] and a large variety of structures [9], [10]. Hereafter, we have adopted some available concepts to be used for e-beam benchmarking purposes e.g. fractal grating [11], [12] and phyllotactic model [13].

The main goal of this contribution is the study and implementation of mathematical methods that can generate highly variable benchmark patterns for e-beam origination of large area grating structures with predefined range of both spacial frequencies and azimuths (both discrete and continuous) with a minimal graphical design effort.

2. METHODS

Single Line and Labyrinth. To exemplify the single line concept, let us consider an optical lens (or a curved mirror) that can be constructed either as a Fresnel construction (concentric zones with variable zone widths) or as an equivalent spiral line. Similarly, an equivalent of a cone surface can be either a set of concentric circles with a constant circle separation (circular grating) or a spiral line with a constant raising gradient. In fact, the line length when the line separation distance is below one micron and the line is filling an area of one inch square might be as high as a mile or even more, so the design freedom is practically unlimited. Just one example among a lot of possibilities is shown in Fig. 1: two parts of a closed-line meander, one of them with an oddity as a sketch of a maze or labyrinth. The count of the oddities might be low and thus unrecognizable by naked eye or the count may be elevated creating intended visible pattern.

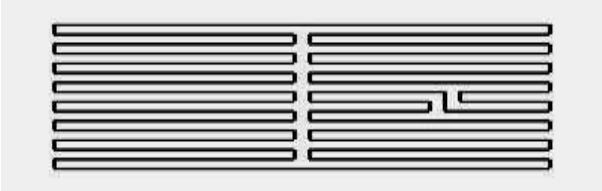

Fig. 1 Single line example – see text for details.

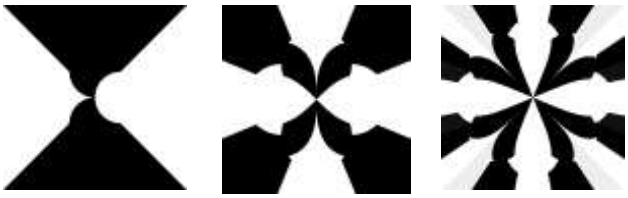

Fig. 4 Forked line origins – see text for details.

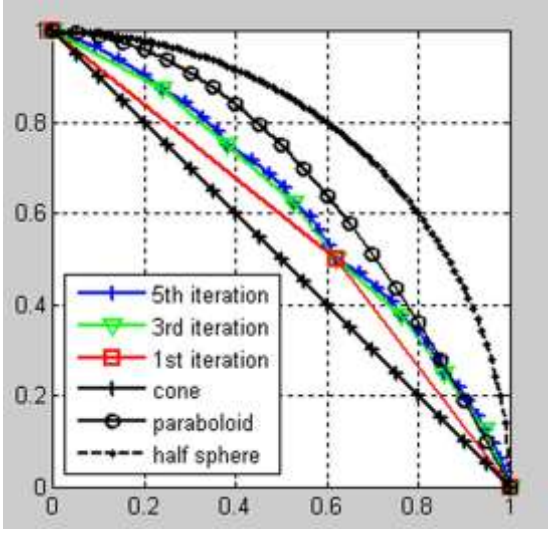

Fig. 2 Fractional relief – see text for details.

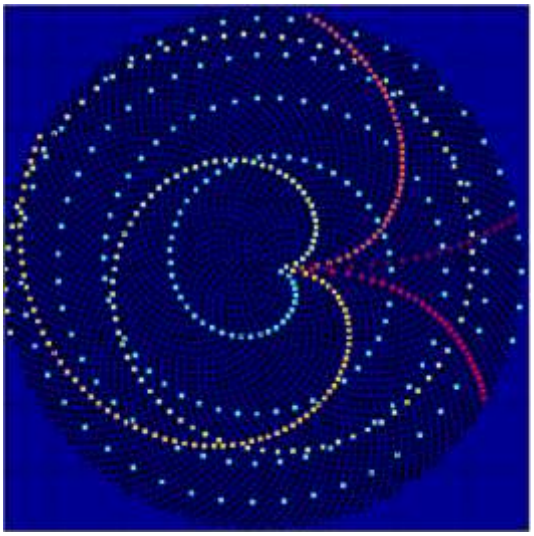

Fig. 3 Filling structure – see text for details.

Area Fractioning. A straight line may be iteratively (***N*** iterations) fractioned to (*e.g.* two) parts by a selected ratio 1 : κ, with $\kappa \neq 1$. Resulting segment widths (for the unity line) range from $(1 / (1+\kappa))^N$ to $(\kappa / (1+\kappa))^N$ giving a span of $N + 1$ discrete segment widths. Such fractioning may be performed in 1D or 2D and using Cartesian or polar coordinates. When adopting the radius 1D fractioning the resulting structure may be regarded to as a virtually volume rotational object. Fig. 2 compares cuts of a resulting structure after few iterations with the cuts of a cone, a paraboloid and a semi sphere.

Tiling and Filling. Some tiling method (e.g. non-orthogonal non-periodic Penrose tiling) may be adopted for benchmarking purposes. The quasi crystal Penrose mesh (with the fivefold symmetry and the underlying long range order) is suitable when quasi discrete frequencies and azimuth are of interest. Also some nature-inspired filling model can be adopted. The phyllotactic model (arrangement of sunflower seeds, [Vogel]) has a sequence of n seed positions expressed in polar coordinates by $[\, r_n \;\; \theta_n] = [\, c \cdot n^{1/k} \;\; n \cdot \theta_0 \,]$, where c is a normalizing factor, $k = 2$ provides the constant filling over all the area (when k is increased, the filling of outer regions become denser and vice versa) and θ_0 is a rotational factor that has to be selected appropriately (the golden angle is a natural compliant choice, but not the unique one). Fig. 3 shows a detail of an inner part of the model with highlighted undersampled subsequences with sampling ratios selected from Fibonacci series.

Forked lines. This method explores the well known approach of self similarities or fractal sequences and objects e.g. Koch snowflake, Haines sphere-flake, Sierpiński sieve, Mandelbrot and Julia / Fatou sets, Barnsley's fern, Dragon curve and many others. Those objects when constructing either from single lines or from forked lines (eventually from both ones) can have very interesting properties for the discussed benchmarking purposes: very large range of spacial frequencies (potentially both discrete and continuous) as well as azimuth of line orientation (again both continuous and/or discrete). As an example one can iterate Mandelbrot quadratic polynomial $z_{n+1} = z_n^2 + c$ in the complex plane with a selected pre/post processing. While the graphic artwork cares of the interpretation of resulting objects (coloring, palette selection, animation, shading, *etc.*), the high resolution patterning device can be used just to delineate (in the simplest case) black lines on a white background resulting in a genesis of self-contained colors and vitality. Fig. 4 shows an interesting origination of the forked line in one of the studied objects: from the initial half space with a singularity (left), through the forking from 2 to 4 lines (middle)

Table 1 Overview of the presented methods

Method	Frequency	Azimuth	Element
Single line — Spiral Lens — Spiral Cone	any continuous, large range constant	any full range, continuous full range, continuous	any line line
Fracturing — Rotational	discrete, large range	full range, continuous	line
Tiling	discrete	discrete	pit
Filling	constant	full range, continuous	pit
Forking	continuous, large range	full range, continuous	line

to the forking from 4 to 8 lines (right). The forking continues further over the structure, all having the same origin and being connected together. As naturally, the spacial frequency range is very large, the initial complex space could be modified such that the given range would decrease. On the other hand, the frequency range can be kept as it is and it could be purposely under sampled at a specific resolution leaving the inner and outer part of the structure with a continual transition from a line structure to randomly spaced pits.

Other Methods. Practically all the described methods can be further combined, masked or extended with large possibilities. Basically, the main line(s) properties (pits properties) such as the width (size), deepness, position variation, tone (positive / negative) can be modified with respect to its Cartesian coordinate. Besides that, the discussed lines (or their segments) and sequences can be regarded as a ordered list of elements; and the mentioned parameters can be modified as a function of the element order within the list. Another interesting variant consist in expanding the input space from 2D to 3D, to adjust the equation and to project the results eventually back to the 2D representation. An overview of the methods is presented in Table 1 – sometimes the classification is not definite; then one variant is specified.

3. EXPERIMENTS, RESULTS AND DISCUSSION

Benchmarking gratings described in the previous chapter were delineated using the e-beam writer. They were adopted to both available system: the Gaussian beam writer EBPG5000plusES with energy of 100 keV and the shaped beam writer BS600+. First, basic entry data formats were evaluating: list of elementary exposures, bitmap format and the vector format. Second, different writing strategies were evaluated seeking for the optimization of the writing speed and the final visual performance. And finally, we prepared benchmark variants with different profile depth and a different line cross section: sine wave profile, steep binary profile and multi-step profile.

Single line structure. A couple of various structures were prepared with different layout, shape and other parameters. As the benchmarking purpose is concerned, we found that Fresnel structures and single line (spiral) structures perform a negligible difference. Fig. 5 shows a difference between a structure delineated with the resolution of 250 nm (on the left) and another one with the resolution of 50 nm (in the middle).The right figure shows a masked elliptical structure incorporated into a ISI ASCR marketing diffraction image. As the resolution comparison is concerned, this is not the only factor influencing the creation of diffraction moiré artifacts shown in the image, but also the sharpness (cross section of the lines) and the kind of filling (lines or pits); *cf* the next paragraph and related images.

Fractional structure. We selected a rotation version with the fraction constant $\varphi = (1 + \sqrt{5}) / 2$ and number of iterations N = 8. Here, we obtain $2^N = 256$ annular segments with N + 1 = 9 distinctive widths. The structure has a design diameter of d = 60 mm. Then, the inner annulus width (or radius of the inner circle) is $(d / 2) / \varphi^N$ and the outer annulus width is $(d / 2) / \varphi^{2\times N}$ being 638.6 µm and 13.6 µm respectively. Further, we cut each annular segment to 93 equally-spaced double zones making the grating period within the zones in the range 6 867 nm down to 146 nm. (We use the term *double zone* in consistency with *the zone* definition in zone plate device.) The resulting structure is shown in Fig. 6. This structure was mainly used for checking the rotational purity of the image and its overall homogeneity.

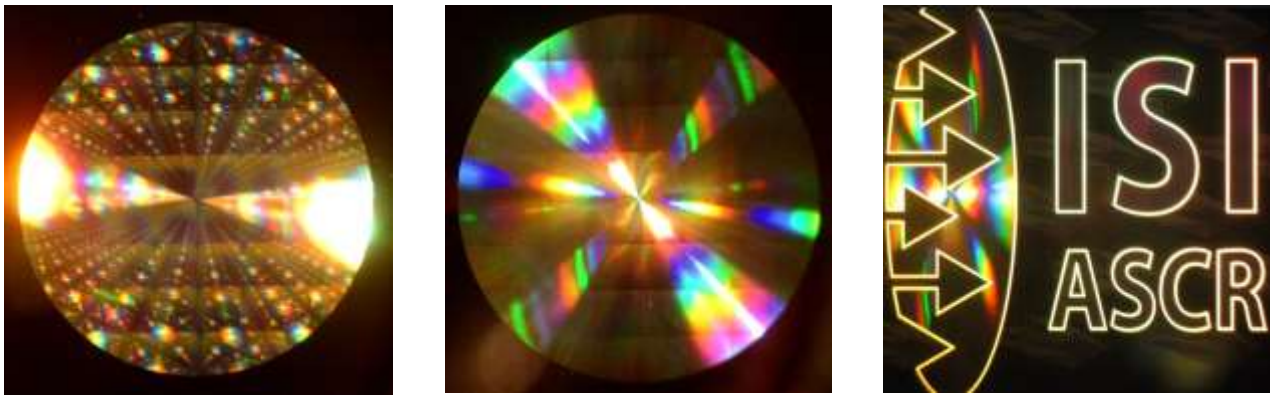

Fig. 5 Fresnel like structures: resolution 250 nm (left), resolution 50 nm (middle), modified structure (right).

Fig. 6 Fractional structure. Photo.

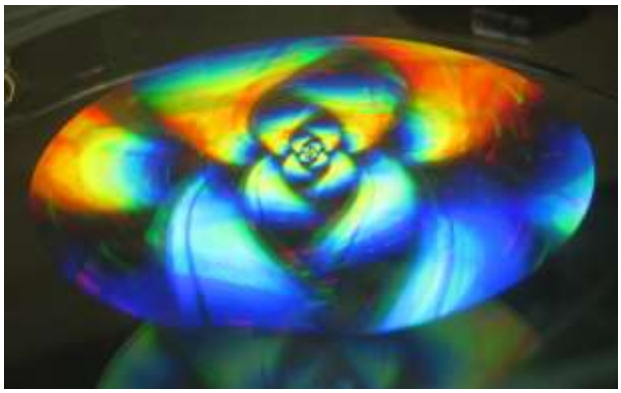

Fig. 7 Filling structure. Photo.

Fig. 8 Filling: rounding the pits position to 50 nm (left) and 1 nm (right). Micrograph, zoom 500×.

Fig. 9 Filling: rounding the pits position to 50 nm (left) and 1 nm (right). Photo, detail.

Filling structure. Here is an example of implementing the filling structure according to equation X. We selected the rotational constant $\psi = 2\pi/\varphi^2$, constant filling ratio, number of pits N = 2.25e9 and outer radius of approximately 30 mm. As the simple algorithm of generating the pits list was very slow, an alternative parallel algorithm was developed allowing the speed up of data generation by the factor of 40. Average spacing between the pits is 1 micron. The image of resulting structure under the wide light source is shown in Fig. 7. The structure has a rotational symmetry meaning that under constant lighting condition the diffractive image remains unchanged when the sample is rotated around the centre. Two different variants of this structure were used to compare the effect of rounding the exact calculated position of the pits. The Cartesian coordinates of each pit were rounded either to 50 nm grid in the first sample or they were rounded to 1 nm grid in the second sample. Moiré structures originated from the first case rounding are well observable under microscope while the pits of the second sample are well regularly spaced (compare the micrograph in the Fig. 8, on the left and on the right respectively). These moiré structures are also visible by the naked eye as it is demonstrated in Fig. 9.

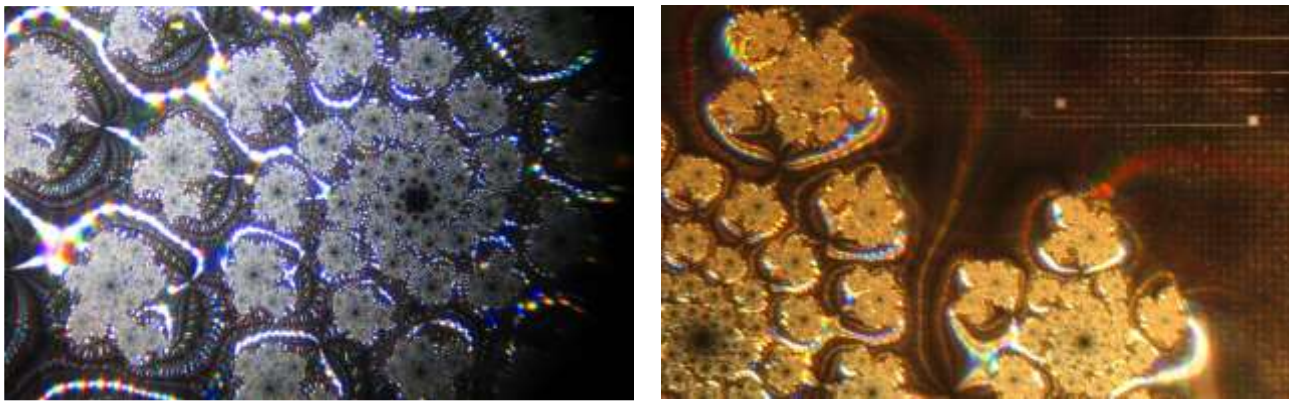

Fig. 10 Forked line structure. Tiny field squaring (0.2 mm) and a few erroneous fields. Magnifying glass.

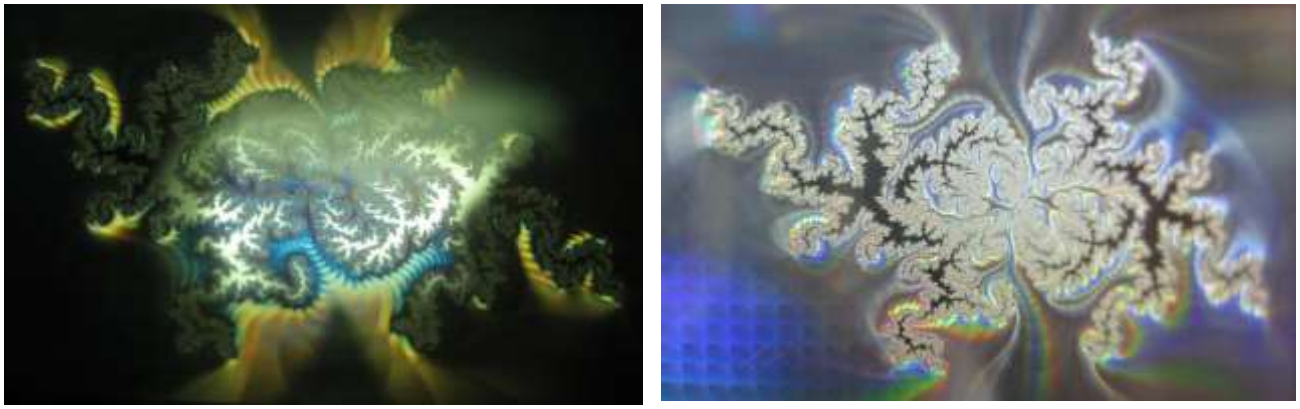

Fig. 11 Forked line: Visible field squaring (2 mm) is observable. Photo.

Fig. 12 Forked line: Some more samples showing the continuity of the lines. Magnifying glass.

Forked lines. Several samples were delineated using the forking line approach. Generally, due to their large range of spacial frequencies (typically 0.1 - 100 μm) they are considered to be very useful for benchmarking purposes. As an example, Fig. 10 shows a sample originated by EBPG writer; the visibility of exposure fields (the image on the right, right upper corner) helped us to adjust data preparation flowchart and the exposure strategy such that the visible squaring practically disappeared in later exposures. Similarly, as shown in Fig. 11 (right image, left lower corner), the sample originated by BS writer exhibits visible squaring. In this case the proper adjustment of writer colon settings and a better selection of beam homogenous area for exposure stamps helped to improve the problem. A few more samples shown in Fig. 12 display improved results without visible issues.

4. CONCLUSIONS

Several approaches to prepare novel kind of gratings were presented. As stated above, they were used as benchmark patterns of e-beam delineation and (both data and process) optimization of diffractive and diffractive-like structures. We assume that these algorithms and structures can be used (alone or in combination with state-of-the-art approaches) in the area of diffractive optically variable image devices. Another potential and exciting application (especially as the forking structures are concerned) might be in visualization of complex models both in live and material sciences where realistic size images with ultimate resolution would be of interest.

ACKNOWLEDGEMENT

This work was supported by MEYS CR (LO1212) together with EC (ALISI No. CZ.1.05/2.1.00/01.0017). The authors wish express their thanks to Mr. Stanislav Král for delineation of structures and magnifying glass documentation as well as to Ms. Dagmar Giričová for photographs.

REFERENCES

[1] RAI-CHOUDHURY, P., *Handbook of Microlithography, Micromachining, and Microfabrication. Volume 1: Microlithography.* Washington: SPIE, 1997. 768 pages. ISBN 0-85296-906-6.

[2] MATĚJKA, F., *Practical E-beam Lithography.* Brno: ISI ASCR, 2013. ISBN 978-80-87441-04-6. *(in Czech)*

[3] KOLAŘÍK, V., *et al.* E-beam Pattern Generator BS600 and Technology Zoom. In *Proceedings of the 4th International Conference NANOCON 2012*. Ostrava: Tanger Ltd., 2012, pp. 822-825. ISBN 978-80-87294-32-1.

[4] BOK, J. *et al.* J. Vac. Sci. Technol. B **31**, 31603-1 (2013).

[5] URBÁNEK, M., *et al.* Shaped E-beam Nanopatterning with Proximity Effect Correction. In *Proceedings of the 4th International Conference NANOCON 2012*. Ostrava: Tanger Ltd., 2012, pp. 717-722. ISBN 978-80-87294-32-1.

[6] MATĚJKA, M., Variable-Shape E-beam Lithography: Proximity Effect Simulation of 3D Micro and Nano Structures. In *Proceedings of the 4th International Conference NANOCON 2012*. Ostrava: Tanger Ltd., 2012, pp. 729-732. ISBN 978-80-87294-32-1.

[7] URBÁNEK, M., *et al.* Monte-Carlo Simulation of Proximity Effect in E-beam Lithography. In *Proceedings of the 5th International conference NANOCON 2013*. Ostrava: TANGER Ltd, 2013, pp. 723-726. ISBN 978-80-87294-47-5.

[8] KRÁTKÝ, S., *et al.* Comparison of Ultimate Resolution Achieved by E-beam Writers with Shaped Beam and with Gaussian Beam. In *Proceedings of the 5th International conference NANOCON 2013*. Ostrava: TANGER Ltd, 2013, pp. 392-398. ISBN 978-80-87294-47-5.

[9] HORÁČEK, V. *et al.* Thin Metallic Layers Structured by E-beam Lithography. In *Proceedings of the 21st International conference METAL 2012*. Ostrava: TANGER, 2012, pp. 993-997.

[10] KOLAŘÍK, V., *et al*. Structural Color of Metallic Surfaces. In *Proceedings of the 23rd International conference METAL 2014*. Ostrava: TANGER Ltd, 2014, 6 pages. *To appear*.

[11] HOU, B., *et al.* Applied Physics Letters. Vol. **85**, No. 25. pp. 6125-6127 (2004).

[12] SKIGIN, D. C., *et al.* Optics Express. Vol. **15**, No. 24. pp. 15628-15636 (2007).

[13] VOGEL, H., A better way to construct the sunflower head. *Mathematical Biosciences* **44** (44): pp. 179–189. (1979).